AD-A140 263 DEFORMATION OF BIMETALLIC BICRYSTALS OF ALPHA-TI/BETA-TI-13MN(U) POLYTECHNIC INST OF NEW YORK BROOKLYN DEPT OF PHYSICAL AND ENGINEERING METALLURGY C S LEE ET AL. NOV 83 N00014-80-C-0742 F/G 20/2 1/1 NL

UNCLASSIFIED

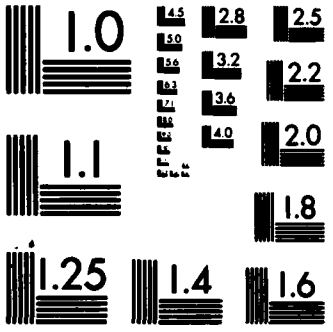

Polytechnic Institute of New York
Department of Physical & Engr. Metall
333 Jay Street
Brooklyn, N. Y. 11201

URG 4

(-7)

Deformation of Bimetallic Bicrystals of α-Ti/β-Ti-13Mn

by

Chong Soo Lee and Harold Margolin

Polytechnic Institute of New York

Brooklyn, N.Y. 11201

Nov. 1983
N00014-80-C-0742

Introduction

Alpha-beta interfaces play an important role in the mechanical properties of α/β (ALPHA/BETA) alloys. These interfaces are the sites of hydrogen segregation and hydride precipitation. In addition there have been a number of investigations which have reported the presence of what has been designated interface phase, and the role of the interface phase on transmitting deformation across the interface has been considered in two separate investigations (1,2). Numerous observations have been made that voids formed at α/β (ALPHA/BETA) interfaces, but voids did not form when slip from α could traverse the interface and pass into the β phase (3). Fatigue cracks have been observed to form and propagate along α/β (ALPHA/BETA) interfaces (4). Catastrophic fracture has also been found to occur at these interfaces (5).

All of these observations attest to the importance of α/β interfaces in controlling properties of α/β (ALPHA/BETA) Ti alloys. Although plastic deformation studies of single crystal α (ALPHA)-Ti have been carried out (6,7-10) and single crystal studies of β (BETA)-Ti have been made (11), no studies, up to this investigation, have been carried out on α/β bimetallic bicrystals. Of particular interest is the question of how compatibility is maintained between the two phases.

Experimental Procedure

1. Materials, Single Crystal Growth, Bonding Procedure

The Ti-Mn system was selected for use in making the bicrystals components, because it was possible to use high temperatures to produce bonding in a reasonable time period, while still permitting the β phase to be retained on quenching (12). The α-Ti, received as 19mm dia., bar contained 0.053 O, 0.003 C, 0.0026 N and 0.0074 H. The Ti-Mn, received as 12.5mm dia. bar, contained 12.9Mn, 0.089 O and 0.008 N. Coarse alpha grains, approximately 10mm x 7mm x 5mm were grown by cycling through the transformation temperature, 882°C, in a Bridgman furnace. Ti-Mn bars approximately 12.6cm long and 1.27 cm in dia., were machined wth a 0.1% taper. These bars were pulled to a strain of 3% within a 2.54 cm length at the smaller diameter end. The bars were sealed in argon filled quartz capsules and annealing was begun at 700°C. After 12 hours the temperatures was increased by 50° and this procedure was followed up to 1150°C. Final annealing occurred at 1170°C for 1 week. At 1170°C the pressure of argon was 1 atmosphere. Crystals approximately 10-15mm long and 8.6mm in dia. were frequently obtained with this procedure.

After polishing to produce parallel sides, the specimens were mounted in a clamp. The whole assembly was wrapped in Ti sheet and annealed for a week at 700°C in a vacuum of approximately 1.3×10^{-3} Pa. The assembly was quenched at the end of the bonding period. After disassembly the specimens were immediately reheated to 700°C for ½ hour and water quenched. This procedure was followed to avoid cracking which developed in β, due to omega formation.

A1

Some movement of the β phase toward the α phase was noted, but no recrystallization took place at the interface, unless the clamp was made very tight. The clamp was usually hand tightened and this procedure produced good bonding and no recrystallization.

After bonding, the bicrystal was hand polished through 600x grit and then electropolished in an electroyte containing 500 cc methanol, 30 cc H_2SO_4, 15 cc HF at -55°C. Laue back reflection patterns indicated that the original orientations were maintained after bonding. The specimen dimensions were 7.6mm in height, 6.4mm in width and 4.6mm in thickness. The specimen was compressed in three stages, 0.58%, 2.1% and 4.6% plastic strain, and was examined after each compression.

2. Finite Element Method (FEM) Procedure

A. A three dimensional finite element method program identified as STRUDL II (13) was employed. Each component was divided into 120 rectangular parallelepipeds, which were smaller near the interface and larger away from the interface. The z-axis was vertical and both the z and x axes lay in the interface. The origin at the center of the base was held fixed so that no motion could take place. The surface positions at +x and -x were allowed to move freely in the x directions but were not allowed to move in the y direction. The +y and -y positions at the surface were held fixed in the x direction but could move freely in the y direction. All other positions on the base could move freely in the x and y directions but could not move in the z-direction. The top surface moved uniformly in the z-direction and freely in the x and y direction. All others positons were allowed to move freely in the x, y and z directions.

The elastic constants for α-Ti (14) are C_{11} = 1.624, C_{12} = 0.920, C_{13} = 0.690, C_{33} = 1.807, C_{44} = 0.467, all in units of 10^{11} Pa. The elastic constants for β-Ti, taken from the elastic constants determined for Ti-Cr alloys (15), are C_{11} = 1.331, C_{12} = 0.951, C_{44} = 0.427, all in units of 10^{11} Pa.

These constants were converted to the appropriate values for the α and β orientations. For α the stress axis was $[\bar{1}101]$ and for β the stress axis was $[8\bar{1}\bar{1}2]$. The interface orientation was as follows

$$(\bar{1}103)_\alpha \;//\; (32\bar{1})_\beta$$

$$[11\bar{2}0]_\alpha \;//\; [129]_\beta$$

Results

A. FEM Calculations of Resolved Shear Stress

FEM calculations showed that in addition to the applied $\sigma_{z'z'}$ stress, $\sigma_{x'x'}$, $\sigma_{y'y'}$, $\sigma_{x'z'}$, $\sigma_{x'y'}$ and $\sigma_{y'z'}$ stresses were present at the interior of the FEM specimen. Although the $\sigma_{x'z'}$ and $\sigma_{x'x'}$ stresses at the $\pm x'$ surface were considerably smaller at the surface then they were at the interior they were not zero. However, in calculating surface stresses $\sigma_{x'x'}$ and $\sigma_{x'z'}$ were assumed to be zero. The stresses on the center section of this specimen are illustrated in Figs. 1 and 2 for an applied strain of 0.0014, considered to be elastic. Figs. 1a,b show the resolved shear stresses for a number of slip systems at the +x' surface and interior, respectively, of the α component. Figs. 2a,b demonstrate the resolved shear stresses for a number of slip systems at the +x' surface and interior, respectively, of the β component.

Resolved shear stresses for seven slip systems in α are shown in Figs. 1a,b. There are some differences between surfaces and interior particularly near the interface. It is of interest to note that the $(01\bar{1}0)$ $[2\bar{1}\bar{1}0]$ slip system had the lowest resolved shear stress on the surface and in the interior, while the $(10\bar{1}1)$ $[\bar{1}2\bar{1}0]$ slip system had the highest resolved shear stress. For both surface and interior the third highest resolved shear stress slip system was the c+a slip system $(1\bar{1}01)$ $[2\bar{1}\bar{1}\bar{3}]$.

For the β component resolved shear stresses for nine slip systems are shown. For both the surface and interior there is a tendency for the resolved shear stress to be highest at the interface. The three slip systems with the highest resolved shear stresses are the $(1\bar{2}3)$ $[\bar{1}11]$, $(1\bar{1}2)$ $[\bar{1}11]$ and $(0\bar{1}1)$ $[\bar{1}11]$ all with the same slip direction. The order of resolved shear stress changes from surface to interior for the second and third highest resolved shear stress slip systems. For both α and β components the surface and interior stresses differ by about 10%.

B. Identification of Slip and Twinning in α-Ti

1. Slip

Fig. 3 shows photomicrographs in the vicinity of the interface of the upper, center and lower portions of the bicrystal after a plastic strains of 4.6%. The indicated slip traces have been identified by single surface analysis. Near the interface the following c+a slip systems have been identified: $(1\bar{1}01)$ $[2\bar{1}\bar{1}3]$, $(\bar{1}2\bar{1}2)$ $[\bar{1}2\bar{1}\bar{3}]$ and $(01\bar{1}1)$ $[\bar{1}2\bar{1}\bar{3}]$. The latter two slip systems cross slip, and, therefore, their identification is unambiguous. Although the $(1\bar{1}01)$

slip plane includes on a -direction the possible resolved shear stresses would be too low to operate such a slip system. Away from the interface $(01\bar{1}0)$ $[2\bar{1}\bar{1}0]$ slip was identified, and there is evidence that this slip system and $(01\bar{1}1)$ $[2\bar{1}\bar{1}0]$ cross slip. This makes a total of five identified slip systems.

Fig. 4 is a higher magnification of a section of Fig. 3c. The location in Fig. 3c can be determined by noting the positions of two identations in the rightside of the boundary of the twin nearest the interface. One of the slip traces adjacent to the α/β interface is marked with a question because it could not be identified with any known slip trace. The slip trace in the $10\bar{1}2$ twins may be due either to pyramidal $\{10\bar{1}1\}$ or $\{11\bar{2}2\}$ c+a slip.

2. Twinning

Five major twinning systems have been identified three of the $\{10\bar{1}2\}$ type and two of the $\{2\bar{1}\bar{1}\bar{1}\}$ type. Three of the twinning systems identified are shown in Fig. 3b. Two $\{10\bar{1}2\}$ and two $\{2\bar{1}\bar{1}1\}$ twinning systems are revealed in Fig. 5. Fig. 5 demonstrate the formation of ragged twins. The $\{2\bar{1}\bar{1}1\}$ interface with the matrix serves as a nucleating site for $\{10\bar{1}2\}$ twins.

C. Slip in β-Ti-13Mn

At the interface the principal operating slip sysems in β were the $(0\bar{1}1)$ $[\bar{1}11]$ and $(\bar{1}\bar{3}2)$ $[\bar{1}11]$ slip systems. Near the top $(0\bar{1}1)$ $[\bar{1}11]$ tended to predominate and at the center of the β component $(2\bar{1}1)$ $[\bar{1}\bar{1}1]$ slip was noted as well, Figs. 3a,b. Near the bottom the $(\bar{1}\bar{3}2)$ $[\bar{1}11]$ slip tended to be reduced, Fig. 3b. Away from the

interface $(1\bar{1}2)$ $[\bar{1}11]$ and $(1\bar{2}3)$ $[\bar{1}11]$ slip tended to operate. The $(1\bar{2}3)$ $[\bar{1}11]$ slip tended to extend all the way to the interface near the bottom, Fig. 3c. It can also be seen in Fig. 3c that slip has extended, without deviation, into the region where the β has moved into the α as a result of diffusion. This slip behavior confirms that movement of the β phase was not accompanied by recrystallization.

D. Discussion of Bicrystal Results

The critical resolved shear stresses for c+a slip systems have not been determined. However, since they are not frequently observed, it is reasonable to presume that the critical resolved shear stresses for c+a slip systems are considerably above those for $\{10\bar{1}0\}$, $\{10\bar{1}1\}$ and (0001) slip along $\langle 11\bar{2}0\rangle$. Furthermore, the resolved shear stresses on two c+a slip systems, $(\bar{1}2\bar{1}2)$ $[\bar{1}2\bar{1}3]$ and $(01\bar{1}1)$ $[\bar{1}2\bar{1}\bar{3}]$ are so low for the applied stress that they do not appear in Fig. 1a,b. Nevertheless, all these c+a slip systems operated near the interface. Examination of the strains which the $(01\bar{1}0)$ $[2\bar{1}\bar{1}0]$ and the $(1\bar{2}3)$ $[\bar{1}11]$, $(1\bar{1}2)$ $[\bar{1}11]$ and $(0\bar{1}1)$ $[\bar{1}11]$ slip systems produce at the interface indicates that the principal incompatibility is the $\gamma_{x'z'}$ and this arises from the greater $\gamma_{x'z'}$ strain in the α component. The three c+a slip systems act to reduce this incompatibility. The operation of these c+a slip systems indicates that sufficiently high stresses were generated as a result of the plastic incompatibility to cause them to operate. It is possible that the higher flow stresses in the β permitted sufficiently high interaction stresses to develop to cause c+a slip to operate. If this is true, it would explain why c+a slip is not seen in single crystal deformation of unalloyed α-Ti. The overall flow stresses

in each component was determined after the 4.6% plastic strain by removing 42% of the β phase and restraining to just beyond the yield stress again. From the equation $\sigma_T = \sigma_\alpha v_\alpha + \sigma_\beta v_\beta$, where σ_T = the total applied stress, σ_α and σ_β are the flow stresses in α and β, respectively, and v_α and v_β are the volume fractions of α and β respectively, it was possible to calculate the unknown σ_α and σ_β from the two sets of stress-strain data. The flow stress of α was 350Mpa, and the flow stress of β was 909Mpa.

For each of the twinning systems observed to operate it is necessary that each accommodate plastic compression. Each twinning system was analyzed and it was found that they could all produce compression.

Fig. 3b reveals that the $\{2\bar{1}\bar{1}1\}$ twins do not extend all the way to the interface. Presumably this is due to the incompatibility between the strains produced by the twin and the strains produced by the primary slip in β.

It was suggested earlier that Fig. 3 indicates movement of the interface from the β side to the α side. The diffusivity of Mn in β and in α-Ti is higher than the self-diffusivity of Ti in α or in β (16), and the self diffusivity of Ti is higher in β than in α (16). In addition the Mn content of the β phase, 12.9 wt.%, is higher than the β equilibrium composition at 700°C, 11.3 wt.% (17), and, therefore, movement of Mn from β to α and Ti from α to β would be expected. The voids which are seen parallel to the interface are probably the result of incomplete bonding, because there is no correlation between the extent of boundary movement and the presence of voids.

Figs. 3b,c show a tendency for slip to shift from the secondary $(\bar{1}\bar{3}2)$ $[\bar{1}11]$ to the primary slip systems $(1\bar{1}2)$ $[\bar{1}11]$ and $(1\bar{2}3)$ $[\bar{1}11]$. The $(\bar{1}\bar{3}2)$ $[\bar{1}11]$ slip system produces greater $\gamma_{x'y'}$ incompatibility with respect to the $(01\bar{1}0)$ $[2\bar{1}\bar{1}0]$ slip system than do the primary slip systems. However, the $(\bar{1}\bar{3}2)$ $[\bar{1}11]$ slip produces less $\gamma_{x'y'}$ incompatibility with respect to the c+a slip systems, and, perhaps, this is why it operates. It is also evident that the appropriate stress must also be available for the secondary slip system to operate. Thus, the extent from the interface over which the secondary slip operates is an indication of the decay distance over which these secondary stresses are sufficiently high to permit the secondary slip to operate.

It is of interest finally to note that away from the interface the slip systems which operated were those with the calculated highest resolved shear stresses, Figs. 1,2, for both α and β phases. For the α phase the $(01\bar{1}0)$ $[2\bar{1}\bar{1}0]$ slip system has the lowest resolved shear stress, Fig. 1, but it also has the lowest critical resolved shear stress (7-10).

Acknowledgment

This work was sponsored by the Office of Naval Research under Contract No. N-00014-80-C-0742. The authors wish to express their appreciation to Dr. Bruce Mac Donald for continued high interest and encouragement.

References

1. S. Ankem and H. Margolin: Met. Trans. A 1980, vol. 11A, p. 963.

2. C. Hammond and H. Margolin: Joint Report on AFOSR Grant # 79-0028 and ONR Contract # N-00014-75-C-0793, Dec. 1981.

3. M.A. Greenfield and H. Margolin: Met. Trans. 1973, vol. 3, p. 2649.

4. Y.R. Mahajan and H. Margolin: Met. Trans. A 1982, vol. 13A, p. 257.

5. M.A. Greenfield and H. Margolin: Met. Trans. 1972, vol. 2, p. 841.

6. F.D. Rosi, C.A. Dube, B.H. Alexander: Trans. AIME 1953, vol. 197, p. 275.

7. A.T. Churchman: Proc. Roy. Soc. 1954, vol. A226, p. 216.

8. E.D. Levine: Trans. AIME 1966, vol. 236, p. 1558.

9. D.G. Westlake: Trans. AIME 1967, vol. 239, p. 1101.

10. A. Akhtar: Met. Trans. A 1975, vol. 6A, p. 1411.

11. P.A. Albert: Doctoral Thesis, Metallurgy Dept., New York University, 1955.

12. H. Margolin, A. Graviano and L.S. Castleman: Met. Trans. A, 1977, vol. 8A, p. 1494.

13. ICES STRUDL II Engineering Users Manual, vols. 1,2, Users Group Inc., P.O. Box 8243, Cranston, R.I. 02920.

14. C.N. Reid: Deformation Geometry for Materials Scientists, Pergamon Press, New York, 1973, p. 76,2.

15. E.S. Fisher and D. Dever: The Science Technology and Applications of Titanium, Edited by R.I. Jaffee and N.E. Promisel, Pergamon Press, 1968, p. 373.

16. F. Dyment: Titanium '80, Science and Technology, edited by H. Kimura and D. Izumi: TMS-AIME, Warrendale, PA, 1980, vol. 1, p.519.

17. M. Hansen and K. Anderko: Constitution of Binary Alloys, McGraw-Hill Book Co. Inc., 1958, p. 957.

Figures

Fig. 1 a. Calculated Resolved Shear Stresses for Various Slip Systems at the Surface of the α-component of the Bicrystal at an applied elastic strain of 0.0014.

b. Calculated Resolved Shear Stresses for Various Slip Systems at the Inside of the α-component of the Bicrystal at an applied elastic strain of 0.0014.

Fig. 2 a. Calculated Resolved Shear Stresses for Various Slip Systems at the Surface of the β-component of the Bicrystals at an applied elastic strain of 0.0014.

b. Calculated Resolved Shear Stresses for Various Slip Systems at the Interior of the β-component of the Bicrystal at an applied elastic strain of 0.0014.

Fig. 3 Observed Slip After a Plastic Compression of 4.6%; a - Upper Portion of Bicrystal; b - Center Section of Bicrystal; c - Lower Portion of Bicrystal.

Fig. 4 Higher Magnification Photomicrograph of a Portion of Fig. 3c.

Fig. 5 Interface of $\{2\bar{1}\bar{1}1\}$ Twin and Matrix Serving as a Nucleating Site for $\{10\bar{1}2\}$ Twins. Note the sets of $\{2\bar{1}\bar{1}1\}$ and $\{10\bar{1}2\}$ Twins.

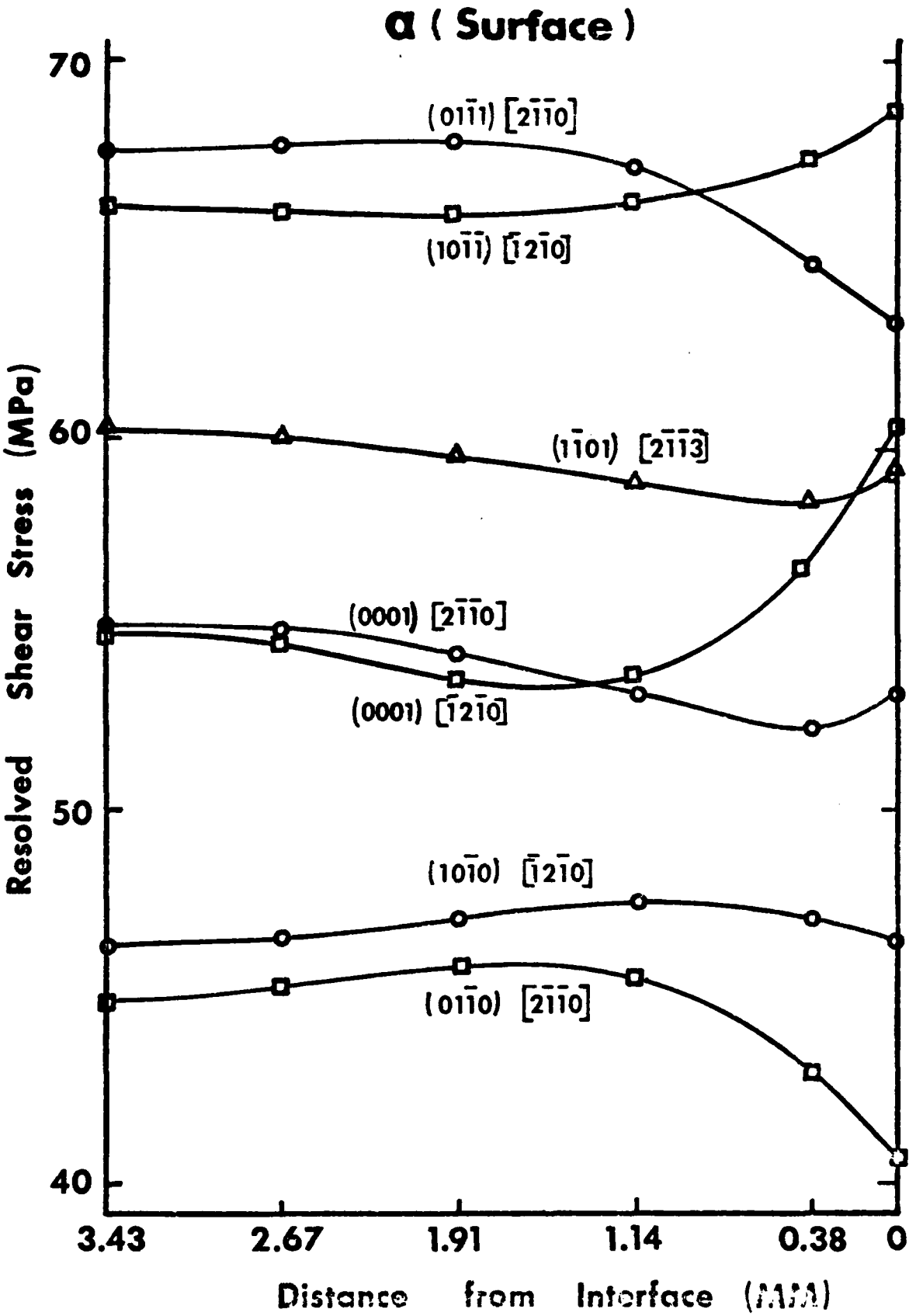

Fig. 1 a. Calculated Resolved Shear Stresses for Various Slip Systems at the Surface of the α-component of the Bicrystal at an applied elastic strain of 0.0014.

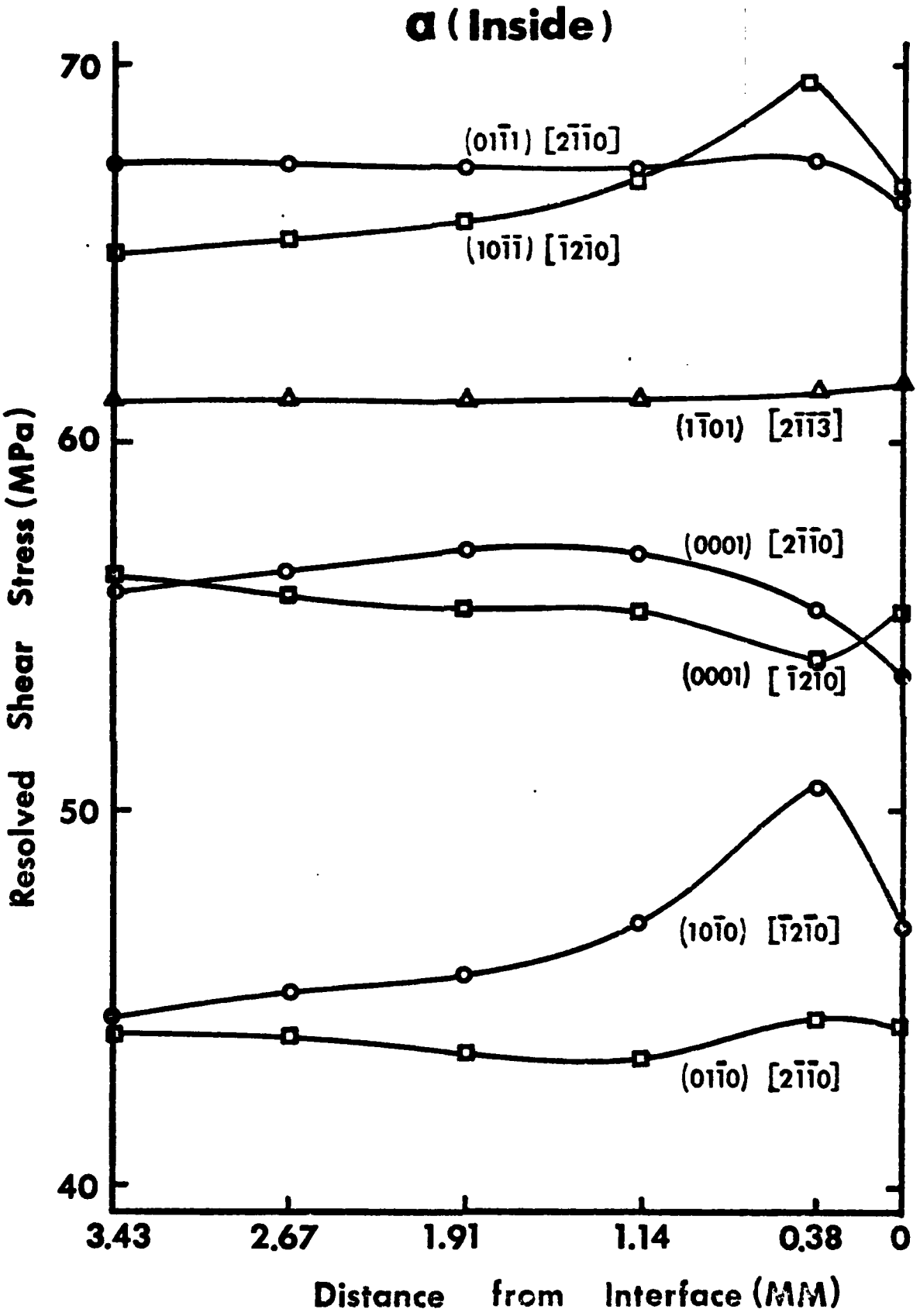

b. Calculated Resolved Shear Stresses for Various Slip Systems at the Inside of the α-component of the Bicrystal at an applied elastic strain of 0.0014.

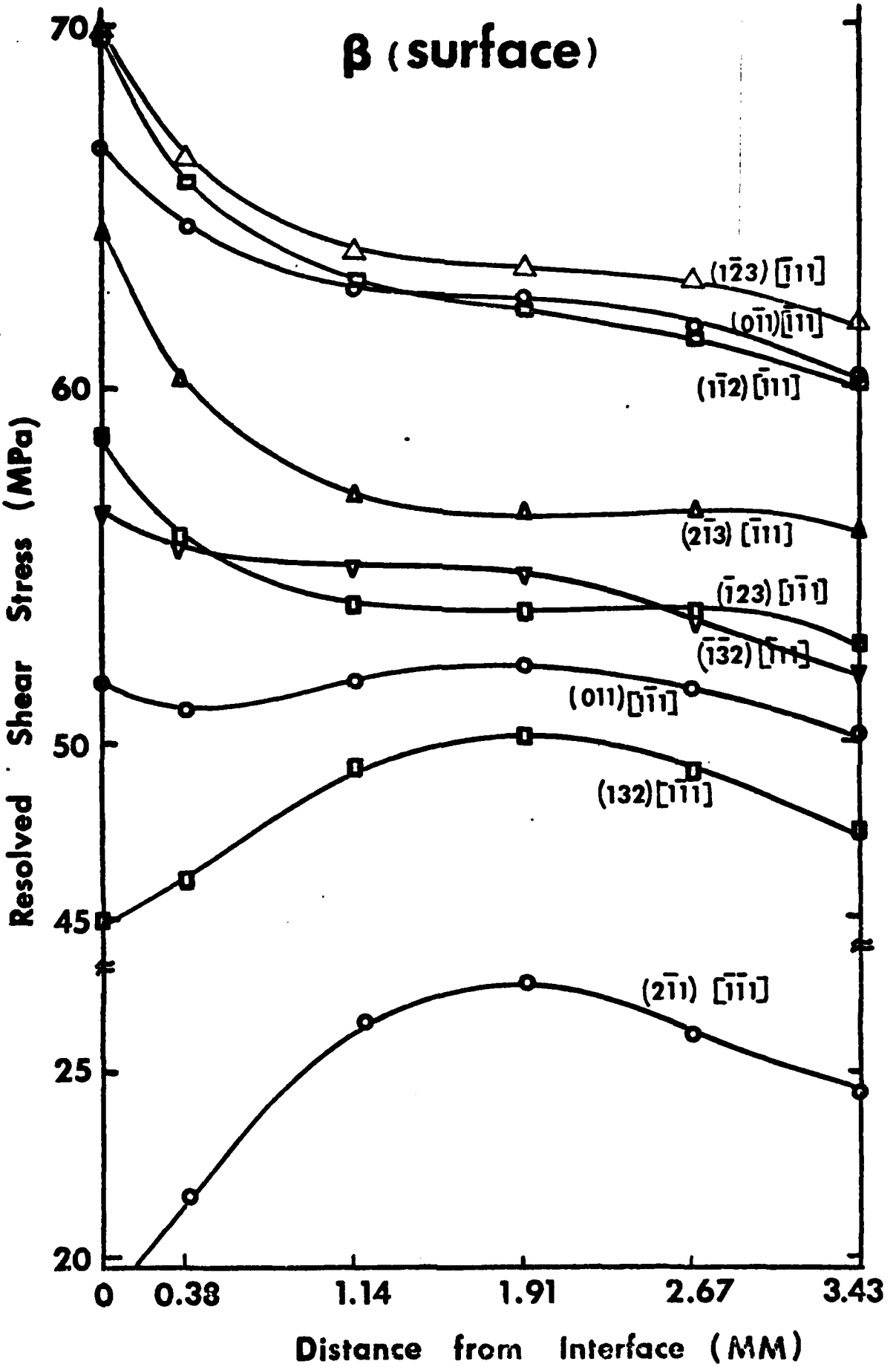

Fig. 2 a. Calculated Resolved Shear Stresses for Various Slip Systems at the Surface of the β-component of the Bicrystals at an applied elastic strain of 0.0014.

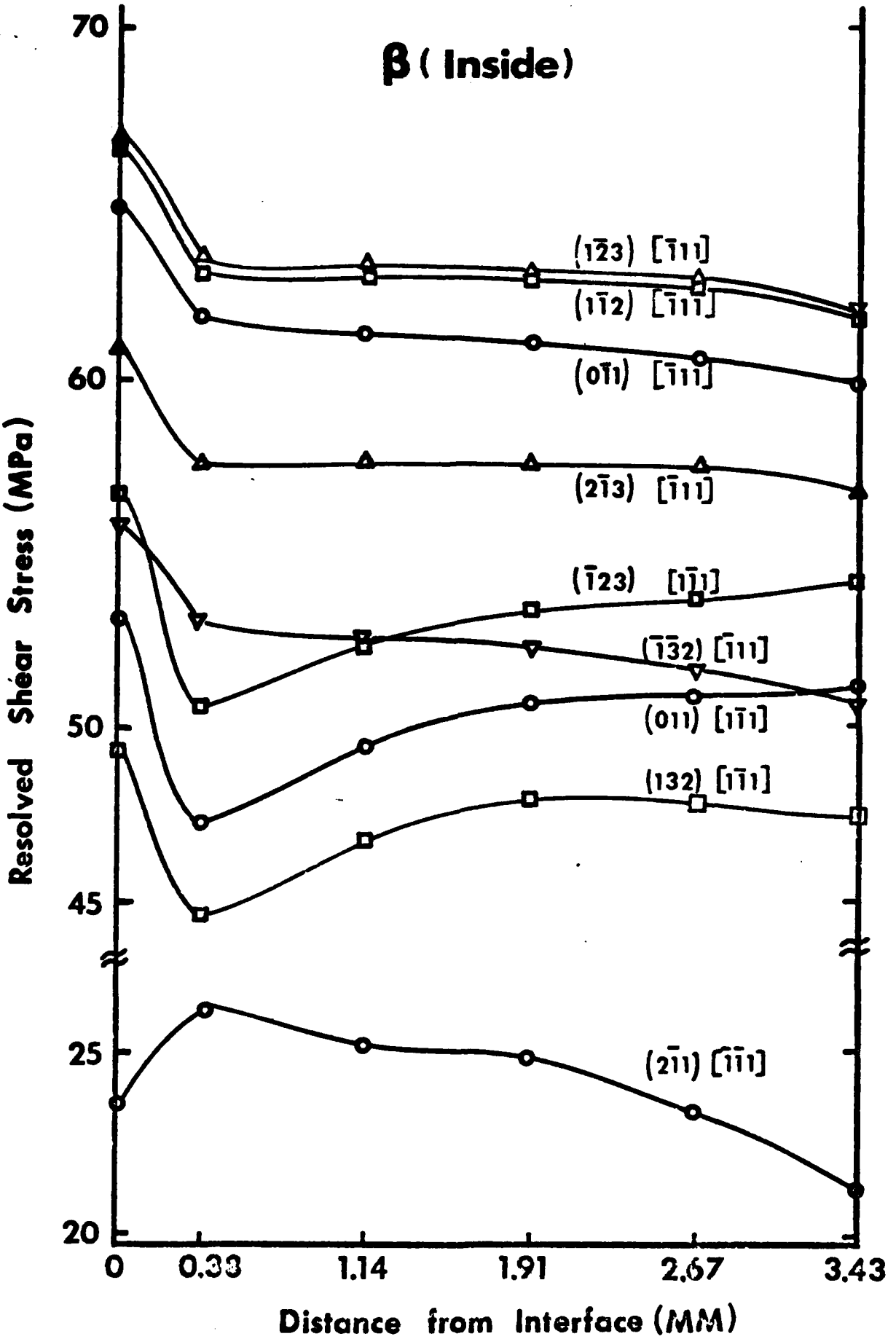

b. Calculated Resolved Shear Stresses for Various Slip Systems at the Interior of the β-component of the Bicrystal at an applied elastic strain of 0.0014.

a

b

c

Fig. 3 Observed Slip After a Plastic Compression of 4.6%; a - Upper Portion of Bicrystal; b - Center Section of Bicrystal; c - Lower Portion of Bicrystal.

Fig. 4 Higher Magnification Photomicrograph of a Portion of Fig. 3c.

Fig. 5 Interface of $\{2\bar{1}\bar{1}1\}$ Twin and Matrix Serving as a Nucleating Site for $\{10\bar{1}2\}$ Twins. Note the sets of $\{2\bar{1}\bar{1}1\}$ and $\{10\bar{1}2\}$ Twins.